PHOTODISSOCIATION DYNAMICS OF THE COLLINEAR VAN DER WAALS COMPLEX $NeBr_2(B,\nu=14\text{-}34)$

DINÁMICA DE FOTODISOCIACIÓN DEL COMPLEJO COLINEAL DE VAN DER WAALS $NeBr_2(B,\nu=14\text{-}34)$

Carlos Andrés Piñeiro Moreno[a], Llinersy Uranga Piña[b,c] and Aliezer Martínez Mesa[c†]

a) Instituto Superior de Tecnologías y Ciencias Aplicadas, Universidad de La Habana, Ave. Salvador Allende y Luaces, Quinta de Los Molinos, Plaza, La Habana 10600. Cuba.
b) Laboratoire Collisions Agrégats Reactivité (FeRMI), Université Paul Sabatier, UMR 5589, F-31062 Toulouse Cedex 09, France.
c) DynAMoS (Dynamical processes in Atomic and Molecular Systems), Facultad de Física, Universidad de la Habana, La Habana, Cuba. aliezer@fisica.uh.cu†
† corresponding author

Recibido 1/8/2024; Aceptado 26/9/2024

We perform trajectory-based simulations of the dissociative dynamics of the collinear van der Waals complex $NeBr_2(B,\nu)$ following photoexcitation to the B electronic state and for varying vibrational excitations of the dihalogen molecule in the range ν=14-34. The quantum dynamics of unimolecular decay is mapped onto a classical-like dynamics in an extended phase space. This methodology allows us to compute the time-dependent dissociation probability, intramolecular energy transfer mechanisms, and transient vibrational state distributions of the linear triatomic system, which are challenging to access experimentally using modern pump-probe spectroscopy techniques. The computed quantities can be used to refine interaction potential models at collinear geometries, which are less well characterized than the T-shaped isomer.

Empleamos simulaciones basadas en trayectorias para estudiar la disociación del complejo colineal de van der Waals $NeBr_2(B,\nu)$, tras la fotoexcitación al estado electrónico B y para distintos niveles vibracionales de la molécula de dihalógeno en el rango ν=14-34. La dinámica cuántica de la reacción unimolecular se describe mediante la evolución temporal de las trayectorias en un espacio de fases ampliado. Esta metodología permite simular propiedades que resultan difíciles de determinar experimentalmente utilizando técnicas modernas de espectroscopía de bombeo-sonda, como la evolución temporal de la probabilidad de disociación y de la distribución de estados vibracionales, así como los mecanismos de redistribución intramolecular de la energía. Los observables calculados pueden utilizarse para refinar los modelos de potencial de interacción para el isómero lineal, que se conoce con menos precisión que para la configuración en forma de T.

PACS: Quantum molecular dynamics (dinámica molecular cuántica), Quantum trajectory method (método de trayectorias cuánticas), Computational physics (física computacional), Molecular physics (física molecular)

I. INTRODUCTION

In recent decades, continuous advances in ultrafast laser spectroscopy have made it possible to investigate dynamical phenomena in atomic and molecular systems across a wide range of time scales [1]. By employing ultrashort laser pulses and delays for improved time resolution, researchers have been able to study phenomena such as chemical reactions and other molecular reorganization processes (occurring typically on the picosecond timescale), molecular vibrations (femtoseconds), and, more recently, electronic phenomena (on the attosecond timescale).

Owing to the complexity of transient absorption spectroscopy signals, elaborate computer simulations are often required to unravel the underlying atomic motion. Nowadays, highly accurate numerical simulations are computationally feasible for physico-chemical phenomena where nuclear motion can be treated classically. Nevertheless, the computational cost of rigorous quantum dynamics simulations (e.g., based on wave function representations using large spatial grids or basis sets) increases exponentially with system size, limiting their applicability to molecular systems with only a few degrees of freedom [2].

Consequently, the development and benchmarking of novel computational methods for quantum molecular dynamics has become a topic of increasing interest. In this context, trajectory-based approaches are particularly attractive due to more favourable scalability compared to quantum wave packet propagation techniques. Additionally, the use of familiar concepts from classical mechanics facilitates intuitive interpretation of the results.

In addition to approximate methodologies, such as semiclassical and hybrid quantum-classical propagation schemes [3], exact reformulations of quantum mechanics in terms of trajectories have been proposed. The coupled harmonic oscillators representation introduced in Ref. [4], and the quantum trajectory method [5], are prominent examples of the latter approach. In Ref. [6], for example, these two methodologies have been combined to study the vibrational predissociation dynamics of the triatomic van der Waals complex $ArBr_2$.

Van der Waals aggregates are widely used as model systems to study energy redistribution mechanisms and the

role of intermolecular interactions. Among these, triatomic dihalogen-rare gas complexes such as $RgBr_2$, RgI_2, $RgICl_2$ (Rg = He, Ne, Ar) have been extensively investigated experimentally and theoretically [7]. Linear and T-shaped isomers of rare gas-halogen complexes exhibit similar stability in the ground electronic state. However, most studies have focused on the T-shaped isomers due to their more intense experimental signals and longer lifetimes compared to the corresponding linear isomers, facilitating detection of the former [8]. Hence, a wealth of information is available on the vibrational and electronic predissociation mechanisms starting from T-shaped structures, while information on the linear isomers remains scarce.

The aim of this paper is to investigate the dissociation dynamics of the linear isomer of the van der Waals complex $NeBr_2(B,v)$ following photoexcitation to the B electronic state of the dihalogen. To this purpose, we considered initial vibrational excitations in the range v=14-34, spanning the range of Br_2 vibrational levels which are experimentally accessible using modern ultrafast laser spectroscopy techniques. The present methodology has been extensively benchmarked in stringent test systems (see [6], and references therein). The present simulations provide insight into the lifetimes and the dissociation pathway of the collinear $NeBr_2(B,v)$ complex, which is difficult to obtain experimentally due to the aforementioned unfavourable spectroscopic signal intensity (compared to that of the T-shape isomer).

The paper is organized as follows. In section Methodology, we describe the main aspects of the 2-fold mapping of the ultrafast quantum dynamics, and the numerical details of the implementation. In section Results, we present and discuss the results concerning the dissociation probability and time scale, as a function of the initial vibrational excitation. The main findings are summarized in section Conclusions.

II. METHODOLOGY

We use Jacobi coordinates (r, R) to specify the configuration of the collinear $NeBr_2$ complex, where r is the Br-Br distance, and R is the separation of the Ne atom from the centre of mass of the Br_2 molecule.

Following Refs. [6, 9], the photoinduced dynamics of the van der Waals complex is described in an effective phase space $\{q_1, ..., q_L,\ p_1, ..., p_L,\ R_1, ..., R_N,\ P_1, ..., P_N\}$, and it is governed by the Hamiltonian:

$$\begin{aligned}\mathcal{H} &= \sum_{nm}\left[\left(\hat{H}_{Br_2}\right)_{nm} + \frac{1}{N}\sum_i W_{nm}(R_i)\right](q_n q_m + p_n p_m) \\ &+ \frac{1}{N}\left[\sum_i \frac{P_i^2}{2\mu} + Q(R_1, ..., R_N)\right] \quad . \end{aligned} \tag{1}$$

Hereafter, $\{q_n, p_n\}$, $n \in [1, L]$ are the generalized coordinates and conjugate momenta of a set of oscillators associated to each of the $L = 40$ lowest lying vibrational states of the dihalogen molecule. R_i denotes the position of the i-th element of a set of $N = 200$ quantum trajectories spanning the region occupied by the probability density distribution along de van der Waals mode, and P_i is the corresponding conjugate momentum. The quantum potential Q and its first derivative, the quantum force, are computed within the Interacting Trajectory Representation (ITR) [10].

In equation (1), $(H_{Br_2})_{nm}$ and $W_{nm}(\hat{R})$ are the matrix elements of the Hamiltonian of the isolated Br_2 molecule, and of the van der Waals interaction $W(r, R)$ between the Br_2 molecule and the Ne atom, respectively. The Br_2-Ne interaction potential in the ground electronic state is described through Morse-van der Waals functions fitting ab initio data for the triatomic complex, whereas in the B electronic state it is modelled as a supperposition of Morse functions representing pairwise Br-Ne interactions [11]. Likewise, the Br-Br interaction in the B electronic state is modelled as a Morse potential:

$$V_{Br-Br}(r) = D\left[e^{-2\alpha(r-r_e)} - 2\, e^{-\alpha(r-r_e)}\right], \tag{2}$$

with parameters $D = 3788$ cm^{-1}, $\alpha = 2.045$ Å^{-1}, $r_e = 2.667$ Å.

The Hamiltonian $\mathcal{H}$ is used to derive the canonical equations of motion in the $2(L + N)$-dimensional phase space, which are solved numerically using the fourth order Adams-Moulton predictor-corrector method with an adaptive time step and relative error tolerance of 10^{-10}, started with the fourth order Runge-Kutta algorithm.

The initial conditions for the propagation are set as follows:

$$\begin{aligned} q_n(0) = \sqrt{2}\delta_{nv}, \quad p_n(0) = 0, \quad n &= \overline{0, L-1} \\ R_{i+1} = R_i + \frac{1}{N\rho_0(R_i)}. \quad i &= \overline{1, N} \end{aligned} \tag{3}$$

This selection corresponds to the initial excitation of the vibrational level v of the Br_2 molecule, while the initial positions of the quantum trajectories reproduce the probability density distribution $\rho_0(R)$ of the ground vibrational state along the van der Waals mode. The ground state density $\rho_0(R)$ is obtained from the solution of the time-independent Schrödinger equation in the ground electronic state, using a Householder reduction algorithm with implicit shifts [12]. The initial momenta P_i of the quantum trajectories are set to zero.

The time evolution of the phase space point is formally equivalent to the solution of the time-dependent Schrödinger equation within the time-dependent Hartree approximation [9].

The time-dependent occupation probability of the vibrational level n is

$$|c_n(t)|^2 = \frac{1}{2}\left(q_n^2 + p_n^2\right). \tag{4}$$

For each initial vibrational level v, the $|c_n(t)|^2$ curve is fitted to a decaying exponential function in order to extract the lifetime τ of the initial state. In addition to the characteristic time scale $\tau(v)$, the vibrational population dynamics provides information on the vibrational relaxation pathways following photoexcitation.

At each point in time, the dissociation probability is computed by integrating the distribution of trajectories beyond a predefined distance R_{max} = 10 Å in the asymptotic region where the potential vanishes. Within the ITR, this integral is equivalent to summing over all trajectories with positions $R_i(t) > R_{max}$.

$$P_d^{(\nu)}(t) = \frac{1}{N}\sum_{i=1}^{N} H\left(R_i(t) - R_{max}\right), \tag{5}$$

where $H(x)$ is the Heaviside step function.

III. RESULTS AND DISCUSSION

III.1. Vibrational energy redistribution

In figure 1, we show the decay time τ of the initial vibrational state of the dihalogen in the collinear $NeBr_2$(B,ν) complex, as a function of the initial vibrational quantum number ν. It can be seen, that the decay of the initially photoexcited vibrational state occurs three orders of magnitude faster for the linear isomer, compared to the typical lifetimes of the same vibrational states in T-shaped $NeBr_2$ complex undergoing vibrational predissociation. Indeed, the experimental measurement of the predissociation lifetimes of T-shaped complexes yielded values between 84 ps and 15 ps, for increasing initial vibrational quantum numbers from ν = 16 up to ν = 29 [13]. Such disparity indicates that the relaxation mechanism of collinear $NeBr_2$ complexes is that of direct dissociation rather than vibrational predissociation.

Moreover, the decay of the initial vibrational state takes place progressively faster for increasing vibrational excitation.

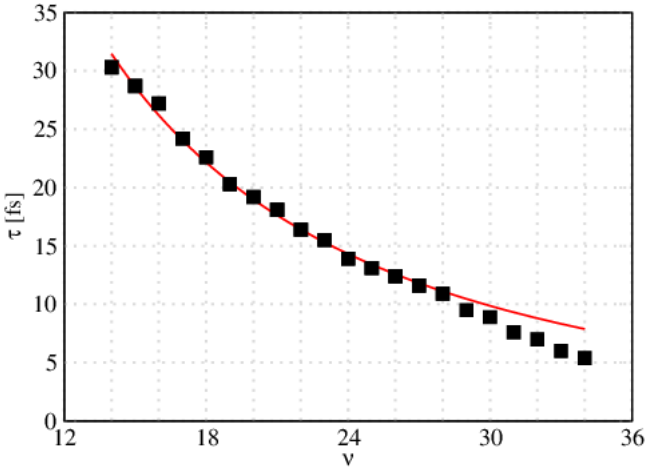

Figure 1. Decay time $\tau(\nu)$ of the initially photoexcitated vibrational state ν of the collinear $NeBr_2$(B) complex (squares). The red curve represents the best fit of the data in the range $\nu = 14-28$ to the functional form $\tau(\nu) \sim \exp(-\kappa\nu)/\nu$.

Inserting the expansion of the van der Waals interaction potential around the equilibrium bond distance r_e of the dihalogen molecule,

$$W(r,R) \approx W(r_e,R) + \left(\frac{\partial W}{\partial r}\right)_{r_e}(r - r_e), \tag{6}$$

into Fermi's Golden Rule, we obtain the following expression for the energy width Γ_ν of the vibrational level ν:

$$\Gamma_\nu \approx \frac{2\pi}{\hbar}\sum_{\nu'}\left[\Theta_W(\nu)\right]^2 \left|\langle\nu'|\left(r - r_e\right)|\nu\rangle\right|^2. \tag{7}$$

Here, the symbol $\Theta_W(\nu)$ stands for the integral over R of the product of three functions, namely the initial and final wavefunctions along the van der Waals mode, and $\left(\frac{\partial W}{\partial r}\right)_{r_e}$. The sum in expression (7) is dominated by the dipole matrix elements coupling the initial state to the nearest neighbouring vibrational levels $\nu + 1$ and $\nu - 1$.

For low enough vibrational levels $\nu \ll \sqrt{2m_{Br}D}/(\hbar\alpha) = 65.5$, the ν-dependent quantities in equation (7) behave as $\Theta_W(\nu) \approx \exp(-\kappa\nu)$, and $\langle\nu \pm 1|(r - r_e)|\nu\rangle \approx \nu$ [14]. Actually, it can be seen that the data closely follow the anticipated curve $\tau(\nu) \sim \Gamma_\nu^{-1} \sim \exp(-\kappa\nu)/\nu$ for vibrational quantum numbers up to $\nu = 28$, and deviates from this functional form for $\nu \geq 29$.

Furthermore, the coupling of the initial vibrational state ν to the level $\nu + 1$ is slightly larger than the coupling to the level $\nu - 1$, due to the progressive reduction of the energy level spacing of a Morse oscillator for increasing ν. Therefore, the early dynamics of the photoexcited $NeBr_2$(B,ν) complex consists of:

i) the exponentially decay of the initial state within the time scale τ,

ii) the concomitant population of the vibrational levels $\nu + 1$ and $\nu - 1$ to a rather similar extent, with a slightly larger transition rate to the former.

Beyond the characteristic time scale τ, the coupling between the states $|\nu \pm 1\rangle$ to their neighbouring energy levels leads to an intricate vibrational energy redistribution process involving many levels. This picture is confirmed by a representative example of the vibrational population dynamics of the linear $NeBr_2$ complex upon photoexcitation of an intermediate vibrational state (ν = 23), displayed in figure 2.

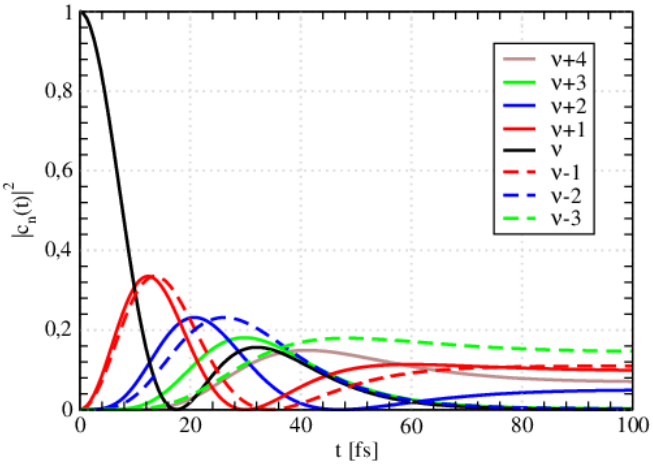

Figure 2. Time-dependent populations $|c_n(t)|^2$ of vibrational states of Br_2 upon photoexcitation of the collinear $NeBr_2$(B,ν = 23) complex.

In this specific example, the initial vibrational state decays completely within the first 17 fs after the photoexcitation,

populating the vibrational levels $v = 24$ and $v = 22$. The latter reaches a maximum population of 33 %, and subsequently transfer it to vibrational levels $v = 25$, $v = 21$, and back to the initial state $v = 23$. The upcoming vibrational energy redistribution involves further closely-lying vibrational states, and the populations tend to stabilise after 100 fs.

III.2. Dissociation dynamics

The time evolution of quantum trajectories $R_i(t)$ upon photoexcitation is shown in figure 3, for the lowest (v=14) and the highest (v=34) initial vibrational quantum numbers considered here. The early quantum trajectory dynamics confirms that, conversely to the T-shape isomer, the photoexcited collinear $NeBr_2(B,v)$ complex relaxes via direct dissociation.

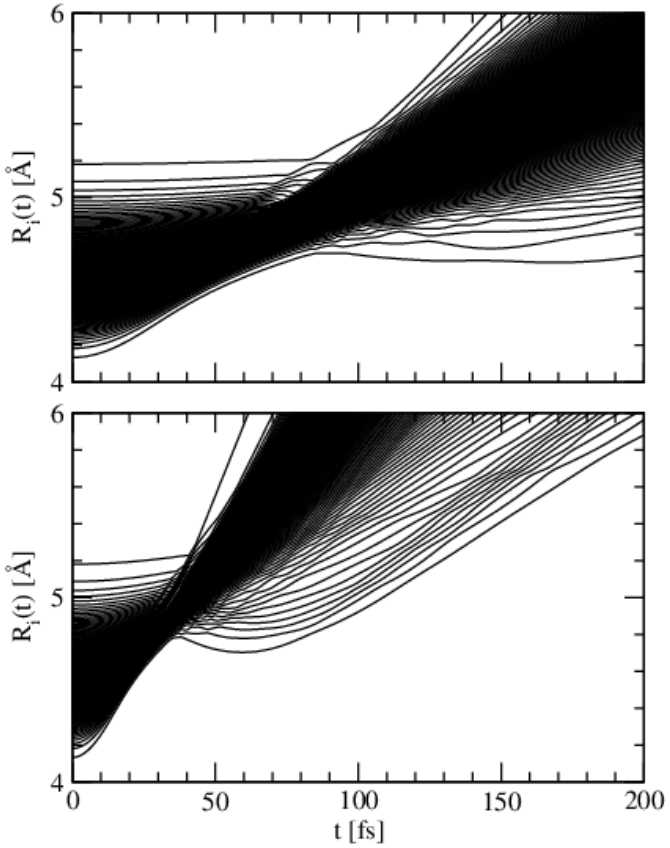

Figure 3. Time evolution of the interacting trajectories $R_i(t)$, for the collinear $NeBr_2(B,v)$ complex, displaying the onset of the dissociation process upon photoexcitation of the vibrational levels $v = 14$ (top panel), and $v = 34$ (bottom panel).

The dissociation mechanism is similar for the two initial vibrational states represented in figure 3. First, the short-range repulsive forces between the Ne atom and the halogen moiety sets the inner quantum trajectories in motion while the outer trajectories remain fairly unaffected, thereby causing the overall distribution to get squeezed. The subsequent expansion of the swarm of trajectories is driven by the repulsive quantum force between neighbouring trajectories, and is characterized by a continuous growth of the centroid position of the distribution along the van der Waals mode.

The sensitivity of the time scale of the dissociation process to variations of the initial vibrational quantum number is apparent in figure 3. For the range of vibrational levels of the Br_2 molecule considered here ($v = 14 - 34$), the probability density distribution along the stretching mode r is chiefly concentrated around the classical turning points. Therefore, in the collinear van der Waals agregate, increasing vibrational excitation causes the reduction of the average distance between the rare gas atom and the closest Br atom. Thus, the mean field potential $W_{vv}(R)$ is steeper at short range for the higher excited vibrational states of the Br_2 molecule. The enhanced repulsion for larger v is responsible for driving the dissociation process faster.

The time-dependent dissociation probability (equation (5)) is plotted in figure 4. The $P_d^{(v)}(t)$ curves look like smoothstep functions. They show that the higher the initial vibrational excitation, the faster the dissociation process. In analogy with the exponential decay, we define the dissociation time scale τ_d as the time elapsed until the dissociation probability reaches 0.632. It can be seen, that $\tau_d(v)$ decreases linearly with the initial vibrational quantum number v, and it is between 30 and 50 times larger than the corresponding lifetime of the initial vibrational state.

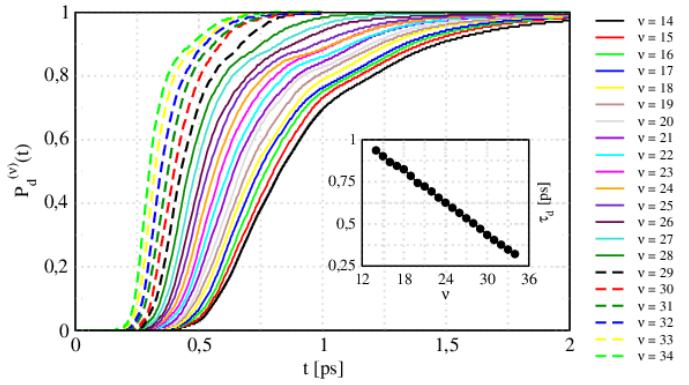

Figure 4. Dissociation probability $P_d^{(v)}(t)$ of the Ne atom from the collinear $NeBr_2(B,v)$ complex. At each point in time, the dissociation probabilities strictly abide the inequalities $P_d^{(34)}(t) > P_d^{(33)}(t) > .... > P_d^{(15)}(t) > P_d^{(14)}(t)$. The dissociation time $\tau_d(v)$ is shown in the inset.

IV. CONCLUSION

We report computer simulations of the photoinduced dissociation dynamics of collinear $NeBr_2(B,v)$ van der Waals complex, for a wide range of initial vibrational states ($v = 14 - 34$) of the dihalogen. The calculations provide insight on the vibrational energy redistribution and on the dissociation pathway of the title system, whose dynamical properties can be difficult to measure using modern transient pump-probe spectroscopy experimental set-ups [8].

Upon photoexcitation, the initial vibrational state v decays on a time scale $\tau \leq 30$ fs. The computed decay times follows the law $\tau(v) \sim \exp(-\kappa v)/v$ for vibrational quantum numbers up to $v = 28$. For higher vibrational states (i.e., $v \geq 29$), this functional form underestimates the transition rate. The

decay of the initial state triggers a complex vibrational energy redistribution process involving several neighbouring levels.

The interacting trajectory dynamics and time-dependent photodissociation probabilities display the direct character of the process. The dissociation time τ_d decreases linearly for increasing initial vibrational quantum number v. The dissociation dynamics is sensitive to the initial vibrational state, yet it proceeds over a much longer time scale than the vibrational dynamics, attaining 100 % quantum yield after $\tau_d \gtrsim 1$ ps.

Contrarily to T-shape isomers undergoing predissociation, the photodissociation of collinear $NeBr_2$ complex is not driven by the vibrational relaxion of the dihalogen moiety. Because the linear isomer undergoes dissociation over a markedly shorter time scale compared to the T-shape complex, time-based discrimination may enable experimental detection of the former using time-resolved spectroscopy. Comparison of the results of numerical simulations as those reported here with the corresponding experimental signals opens the way to fine tune current models of the rare gas-dihalogen, excited-state interaction potentials in the repulsive region, and at linear configurations.

ACKNOWLEDGMENTS

The results incorporated in this publication have received funding from the European Union's Horizon 2020 and Horizon Europe research and innovation programmes, under the Marie Skłodowska-Curie grant agreements n^{o}898663, and n^{o}101155733, respectively.

REFERENCES

[1] M. Maiuri, M. Garavelli, G. Cerullo, J. Am. Chem. Soc. **142**, 3 (2020).

[2] F. Gatti, B. Lasorne, H.-D. Meyer, A. Nauts, *Applications of Quantum Dynamics in Chemistry* (Springer International Publishing, 2017).

[3] T. Nagy, A. Vikár, G. Lendvay, Phys. Chem. Chem. Phys. **20**, 13224 (2018).

[4] J. S. Briggs, A. Eisfeld, Phys. Rev. A **88**, 062104 (2013).

[5] P. K. Chattaraj (Ed.), *Quantum Trajectories* (Taylor and Francis, 2010).

[6] J. C. Acosta-Matos, C. Meier, A. Martinez-Mesa, L. Uranga-Piña, J. Phys. Chem. A **126**, 1805 (2022).

[7] K. C. Janda, Predissociation of Polyatomic Van Der Waals Molecules. Advances in Chemical Physics **60**, 201 (2007).

[8] J. Cabrera, C. R. Bieler, N. McKinney, W. E. van der Veer, J. M. Pio, K. Janda, O. Roncero, J. Chem. Phys. **127**, 164309 (2007).

[9] J. C. Acosta-Matos, A. Martinez-Mesa, L. Uranga-Piña, Chem. Phys. **529**, 110544 (2022).

[10] L. Cruz-Rodriguez, L. Uranga-Piña, A. Martinez-Mesa, C. Meier, Chem. Phys. **503**, 39 (2018).

[11] J. M. Pio, W. E. van der Veer, C. R. Bieler, K. C. Janda, J. Chem. Phys. **128**, 134311 (2008).

[12] W. H. Press, S. A. Teukolsky, W. T. Vetterling, B. P. Flannery, M. Metcalf, *Numerical Recipes in Fortran 90 - The Art of Parallel Scientific Computing* (Cambridge University Press, 1996).

[13] J. A. Cabrera, C. R. Bieler, B. C. Olbricht, W. E. van der Veer, K. C. Janda, J. Chem. Phys. **123**, 054311 (2005).

[14] J. A. Beswick, N. Halberstadt, K. C. Janda, Chem. Phys. **399**, 4 (2012).